



Combustion characteristics of butanol isomers in multiphase droplet configurations



Yu Cheng Liu^{a,*}, Fahd E. Alam^{b,1}, Yuhao Xu^c, Frederick L. Dryer^d, C. Thomas Avedisian^c,
Tanvir I. Farouk^{b,*}

^a Department of Computer Science, Engineering and Physics, University of Michigan – Flint, Flint, MI 48502, USA

^b Department of Mechanical Engineering, University of South Carolina, Columbia, SC 29208, USA

^c Sibley School of Mechanical and Aerospace Engineering, Cornell University, Ithaca, NY 14853, USA

^d Department of Mechanical and Aerospace Engineering, Princeton University, Princeton, NJ 08544, USA

ARTICLE INFO

Article history:

Received 13 October 2015

Revised 20 April 2016

Accepted 20 April 2016

Keywords:

Droplet combustion

Butanol isomers

Biofuel

Numerical simulation

Microgravity

ABSTRACT

This study reports results of experiments on the isolated droplet burning characteristics of butanol isomers (*n*-, *iso*-, *sec*-, and *tert*-) under standard atmosphere conditions in an environment that promotes spherical combustion. The data are compared with predictions from a detailed numerical model (DNM) that incorporates complex combustion chemistry, radiative heat transfer, temperature dependent variable fluid properties, and unsteady gas and liquid transport. Computational predictions are generated using the high temperature kinetic models of Sarathy et al. (2012) and Merchant et al. (2013).

The experiments were performed in a free-fall facility to reduce the effects of buoyancy and produce spherical droplet flames. Motion of single droplets with diameters ranged from 0.52 mm to 0.56 mm was eliminated by tethering them to two small-diameter SiC filaments (~14 μm diameter). In all the experiments, minimal sooting was observed, offering the opportunity for direct comparison of the experimental measurements with DNM predictions that neglect soot kinetics.

The experimental data showed that the burning rates of *iso*- and *sec*-butanol are very close to that of *n*-butanol, differing only in flame structure. The flame stand-off ratios (FSR) for *n*-butanol flames are smaller than those for the isomers, while *tert*-butanol flames exhibited the largest FSR. DNM predictions based upon the kinetic model of Sarathy et al. over-predict the droplet burning rates and FSRs of all the isomers except *n*-butanol. Predictions using a kinetic model based upon the work of Merchant et al. agree much better with the experimental data, though relatively higher discrepancies are evident for *tert*-butanol simulation results. Further analyses of the predictions using the two kinetic models and their differences are discussed. It is found that the disparity in transport coefficients for isomer specific species for Sarathy et al. model fosters deviation in computational predictions against these newly acquired droplet combustion data presented in this study.

© 2016 The Combustion Institute. Published by Elsevier Inc. All rights reserved.

1. Introduction

Liquid fuels have been widely used to power aerospace and ground transportation vehicles. Despite projected decreases in petroleum resources in the future, forecasts suggest that demand for liquid transportation fuel will continue to grow. Liquid fuels are preferred over other forms due to their high energy content, matured engine technologies that utilize them, and fuel manufacturing/distribution infrastructure [1]. In particular, sustainable liquid

fuels derived from biomass (biofuels) have demonstrated potential to be used to augment petroleum derived resources through blending. Creating a self-sustaining, profitable biofuels industry that does not compete with agricultural food supply is a challenge recognized by government mandates in the U.S. and European Union [2,3].


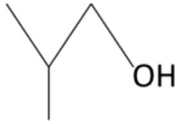
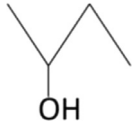
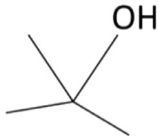
Butanol (C₄H₉OH), as an emerging biofuel, has been identified because of the readiness and continuous development of conversion processes for biomass feedstocks [4]. Selected properties of butanol isomers are shown in Table 1 [5–7]. Butanol isomers have comparatively superior fuel properties, e.g. higher energy density, lower vapor pressure, less corrosive compared to ethanol [6] and also have been considered for use in commercial compression ignition (CI) engines due to their relatively high cetane number [8,9].

* Corresponding authors.

¹ These authors contributed equally to this work.

E-mail addresses: gpits492@gmail.com, franliu@umflint.edu (Y.C. Liu), tfarouk@sc.edu (T.I. Farouk).

Table 1
Selected fuel properties of butanol isomers (C₄H₉OH, M.W. = 78.123 g/mol [9]).

	<i>n</i> -Butanol	<i>iso</i> -Butanol	<i>sec</i> -Butanol	<i>tert</i> -Butanol
Molecular structure				
Liquid density, ρ (kg/m ³) at 298 K ^a	0.81	0.802	0.807	0.787
Liquid viscosity, μ (mPa s) at 298 K ^b	2.544	4.312	3.096	— ^d
Boiling point, T_b (K) ^a	390.9	381	372.7	355.6
Freezing point T_{fr} (K) ^a	183.9	165.2	158.5	298.8
Critical pressure, P_c (atm) ^a	43.6	42.4	41.4	39.2
Research octane number ^b	96	113	101	105
Motor octane number ^b	78	94	32	89
Enthalpy of vaporization, ΔH_f (kJ/kg) at T_b ^b	582	566	551	527
Heat of combustion, $\Delta H_{c,liq}$ (kJ/kg) ^c	–36,087	–36,001	–35,895	–35,669

^a [5].

^b [6].

^c Values converted from [7].

^d *tert*-Butanol is solid at 298 K.

The interests in butanol have attracted much effort towards engine studies. The performance and emission behaviors of both spark ignition (SI) and CI engines fueled by blends of petroleum fuels and *n*-butanol have been extensively reported [10–19]. The addition of *n*-butanol was found to increase the brake specific fuel consumption (bsfc) and brake thermal efficiency [13] and slightly reduce CO and NO_x emissions [10] of diesel engines except for turbo-charged operations [14,15]. In direct injection SI engines, *n*-butanol/gasoline blends promote better anti-knock behaviors and reduction of CO, NO_x and unburned hydrocarbons (UHC) [11]. Pure *n*-butanol combustion has been reported in some homogeneous charged CI (HCCI) engine studies [16,17] and it could increase CO and UHC emissions compared to gasoline in SI engine operations [12]. Regalbuto et al. [18] reported that among butanol isomers, *n*-butanol exhibits the highest NO_x, *iso*-butanol the highest CO, and *sec*-butanol the highest UHC in SI engine experiments. However, Fushimi et al. [19] claimed few isomer effects on NO_x and smoke emission are found in butanol/diesel blend operations.

Oxidation kinetics of butanol isomers have received attention since about a decade ago [20,21]. Development of combustion chemistry of butanol isomers includes a direct comparison with combustion properties measured in configurations that are amenable to detailed numerical modeling (DNM). Currently, such modeling has been widely performed for configurations in which the fuel is pre-vaporized (e.g., jet-stirred reactor (JSR) [22–25], shock tubes [26–29], rapid compression machines/facility (RCM/RCF) [30,31], opposed diffusion flame [32–34] burners, flow reactors [34,35] and pyrolysis reactor and premixed flame probed by a molecular beam mass spectroscopy (MBMS) [21,35–39]). Recently, Sarathy et al. [40] utilized experimental results from MBMS, shock tube, RCM, and JSR configurations to validate a comprehensive oxidation kinetics model for butanol isomers that cover high and low temperature ranges. Van Geem and coworkers [41], Harper et al. [42] and Merchant et al. [43] validated the mechanisms for *n*-, *sec*-, *iso*- and *tert*-butanol pyrolysis and/or oxidation with combustion properties from JSR, opposed flame, laminar flame velocity, and shock tube configurations. This kinetic model has been used in simulating the combustion in more practical systems like a homogeneous charge compression ignition (HCCI) engine [44].

Non-premixed liquid pool ignition experiments [45] of *n*-butanol and *iso*-butanol have been modeled using a reduced version [46] of *n*-butanol oxidation scheme by Sarathy et al. [23] coupled with phase equilibrium parameters. Soot prediction from *n*-heptane/*n*-butanol/PAH mechanisms has also been pursued [47].

However, the performance of the kinetic models developed has not yet been assessed in detailed numerical models of multi-phase combustion configurations that, at the least, may be considered to provide a bridge to spray combustion.

An important attribute of combustion properties obtained from the experimental configurations mentioned above for validating detailed kinetic mechanisms is that those configurations promote a zero or one-dimensional transport process, because doing so significantly reduces computational overhead for modeling while incorporating detail chemistry. However, none of them includes some of the unique multiphase features found in a spray, including fuel vaporization, coupled liquid and vapor transport, moving boundary effects, or the sub-grid spray configuration of droplets. Currently the only combustion configuration that is amenable to detailed numerical modeling which does incorporate such elements is a single isolate droplet burning with spherical symmetry [48–54] such that the droplet and flame are concentric and gas transport is radially symmetric. This paper applies this modeling capability to combustion of butanol isomer droplets under conditions that promote such spherical symmetry.

Experimental studies are noted on butanol isomer droplets at standard [52] and elevated pressures [54–56] as well as under various ambient temperatures [57]. Pure evaporation of *n*-butanol droplets has also been studied [58]. The present study is motivated by the dearth of data for butanol isomers droplet combustion specifically under conditions that promote spherical droplet flames to simplify the transport processes involved as well as representing a multi-phase combustion system. The predicted combustion properties using DNM as described in [50,51] are compared with measurements. Building upon the prior work on *n*-butanol [52], the present study shows both experimental and numerical comparison of droplet burning of all four butanol isomers.

2. Experimental methods

To promote spherically symmetric droplet burning, a combination of low gravity (to minimize buoyancy effects), physically restricting motion of the droplet by tethering it to support structures (to eliminate forced convection) and employing small droplets were used. A gravity level of 10^{–4} g/g₀ was achieved by carrying out the experiments in a laboratory configuration that was in free-fall over a distance sufficient to observe the complete droplet burning history (free-fall over 7.6 m to provide 1.2 s experimental time).

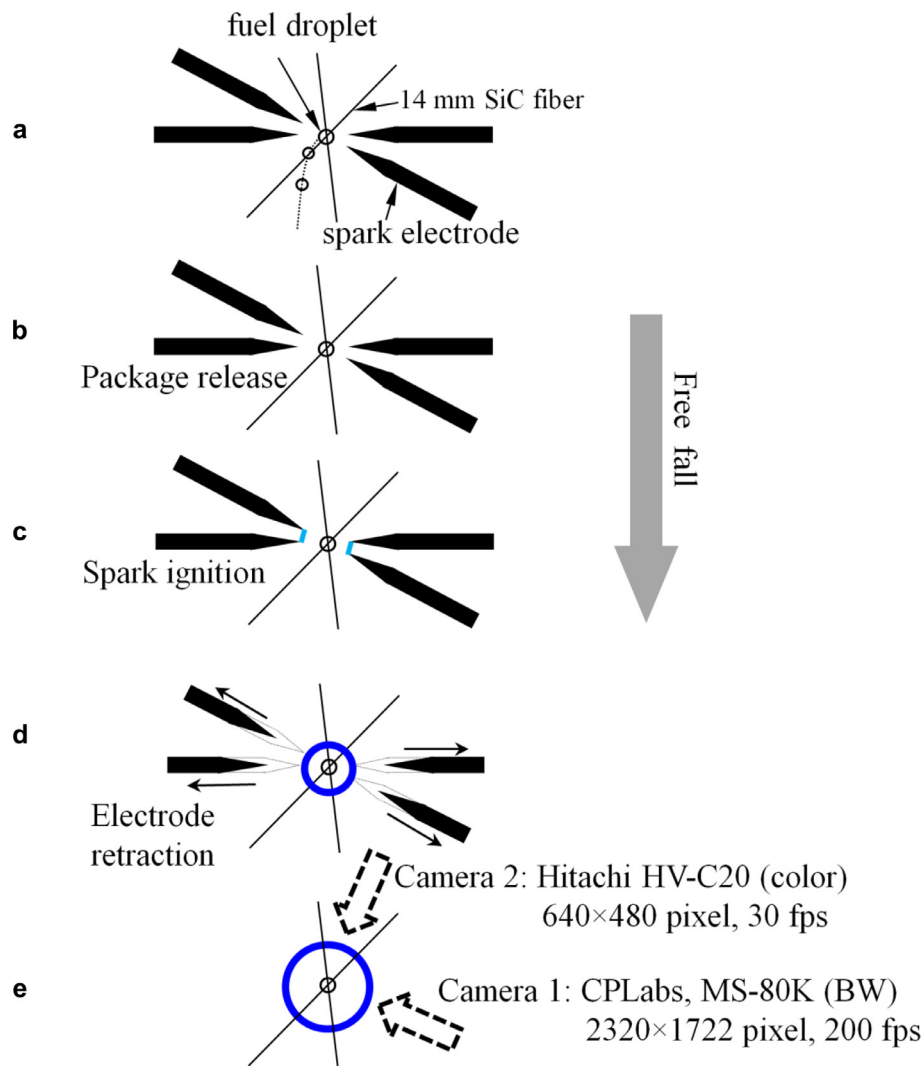


Fig. 1. Illustration of key components and procedures of the experiments: (a) droplet deployment onto the intersection of SiC fiber filaments; (b) package release into free fall; (c) droplet ignition by sparks; (d) electrode retraction; (e) burning history recorded by two cameras.

The details of the experimental setup and procedures can be found elsewhere [59,60] and a brief summary is provided below.

Figure 1 outlines the procedure for the experiment. Test droplets were deployed onto an X-shape configuration of two 14 μm SiC fiber filaments intersecting at 60° (cf. Fig. 1a). Previous work with similar experimental setup shows that the tether fiber has very minimal effects on the data [61]. At the moment the droplet with desired size (~ 0.5 mm) was obtained, the package mounted with combustion chamber, optic systems, and control circuits is released into free fall (cf. Fig. 1b). During free fall, ignition was achieved by spark discharge (cf. Fig. 1c) that is triggered by a multi-channel signal generator and amplified using circuits and power supply on-board the package. Two parallel and symmetrical sparks are fired between electrode pairs positioned on opposite sides of the droplet providing local heat sources to ignite the vapor fuel surrounding the droplet. The electrodes are retracted using current-activated solenoids immediately after the spark discharge to avoid interaction with the spherical droplet flame (cf. Fig. 1d).

A black-and-white (BW) high-speed camera (MS-80 K, Canadian Photonic Labs, 2320×1722 pixel at 200 fps) and a color CCD camera (Hitachi HV-C20, 640×480 pixel at 30 fps) were used to record the history of backlit droplet boundary and color flame, respectively, during the burning process from two different angles (cf.

Fig. 1e). Both cameras are fitted with appropriate telescope lenses, extension tubes and teleconverter for best magnification [61]. The imaging settings including exposure time and lens aperture used in the experiments were identical for all fuels.

For most of the tests conducted in this study, droplet deployment often required more than one droplet coalescence of droplets at the intersection of the fibers to achieve a droplet of the desired size (~ 0.5 mm). Deployed droplets larger than desired were allowed to vaporize down to the desired size. This short vaporization process facilitates development of local fuel vapor concentration near the droplet without changing the overall ambient composition, which is also more favorable to the simulated ignition in modeling. The ambient conditions considered in this study are room temperature and atmospheric pressure air. Among all butanol isomers, *tert*-butanol is particularly problematic. Because of its high melting point ($\sim 25^\circ\text{C}$) it is difficult to transport it into the chamber system and ignite the generated droplets. Slight pre-heating the fuel to about 26°C facilitates those processes prior to the combustion experiments. Once droplets were deployed, no further heating was needed.

All the data presented in this paper were extracted from size measurements of the recorded objects, i.e. droplet from the BW camera and flame from the color camera. With the presence of the

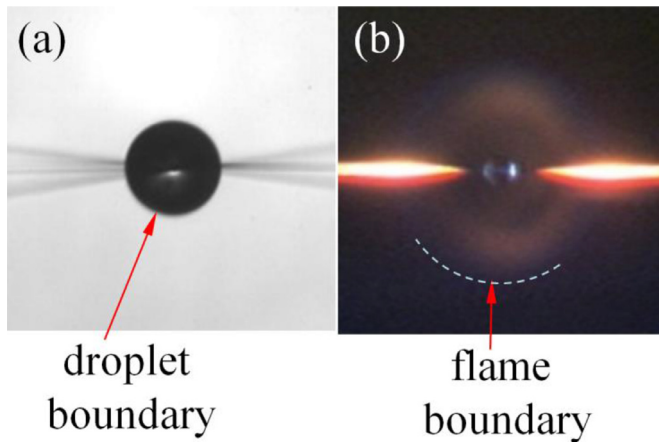


Fig. 2. Representative images from BW (a) and color (b) camera showing the boundaries of droplet and flame.

two support fibers, the shapes of droplet and flame were found to maintain almost spherical (or in a 2D image, circular, see Fig. 2a and b for droplet and flame, respectively). The nature of this type of images allowed using image editing software's basic drawing function to reference and measure the circular boundary sizes.

The isomers were non-sooting under the standard atmospheric pressure conditions of the present experiments. Therefore the recorded BW images all have very sharp droplet boundaries without interferences (cf. Fig. 2a). Droplet diameter (D) measurements were performed using a previously developed MATLAB program that automates the droplet size measurements of sequential BW images [62]. Diameters extracted from this program were sampled and compared with the results from manual operations (using Image-Pro Plus 6.3) to verify the program's reliability. These droplet size data were employed in the D^2 and the flame-standoff ratio plots shown in the results and discussions.

Flame diameters (D_f) were extracted from the video images using the CorelDraw 9 program with a manually placed ellipse positioned around the outer boundary of the luminous zone. The flame diameter extraction process was not automated owing to the more diffuse and less sharp flame boundary. No color adjustments were made for the measurements. Figure 2b shows a flame image of the type involved in applying the CorelDraw 9 software to extract flame diameter measurements (the dotted line is part of an ellipse that represents the flame outer boundary). The flame brightness for all four butanol isomers is very similar. Based on the image shown in Fig. 2b, the boundary of this flame outer edge is considered more uncertain than the droplet size measurement. The uncertainty of flame size measurement is within 4–8 % of the flame size (190 to 100 pixel for the flame size with an 8 pixel uncertainty). The extracted D_f in this paper will be presented as flame standoff ratios ($FSR = D_f/D$) in results and discussions.

The fuels used in the study were obtained from Sigma-Aldrich with the following purities: *n*-butanol, anhydrous, 99.8%; *iso*-butanol, anhydrous 99.5%; 2-butanol, anhydrous, 99.5%; *tert*-butanol, puriss; p.a., ACS reagent, $\geq 99.7\%$ (GC). Selected properties of these fuels are listed in Table 1.

3. Numerical modeling

A recently developed spherically-symmetric multi-component droplet combustion model was used to perform direct numerical modeling (DNM). The description of the model can be found in rigorous details elsewhere [63,64]. The specialty of the model lies in its capability of incorporating detailed gas phase chemical kinetics, spectrally resolved radiative heat transfer, multi-component

transport properties and heat transfer perturbations in presence of the tether fibers. The data correlations of Daubert et al. [65] were used to calculate the liquid phase properties of the condensed fuel.

The present study adapts the thermodynamic parameters, chemical kinetic mechanisms, and transport properties from two separate kinetic sources: 1) Sarathy et al. [40]; abbreviated here as 'LLNL (Lawrence Livermore National Lab)' model; 2) Merchant et al. [43]; the MIT model developed and timely updated by Green and coworkers. The LLNL model used in this paper includes 284 combustion species and 1892 reactions (the high temperature scheme). The MIT model employed here is the Chemkin-II compatible version of Merchant et al. [43] obtained through Green's group at MIT that includes 337 species and 7121 reactions (other than the 373 species and 8723 reactions originally claimed in Ref. [43]).

The complete set of coupled partial differential and algebraic equations are first discretized in space and then integrated in an automated fashion as a set of coupled ordinary differential-algebraic equations in time [63,64]. Spatial discretization is performed according to a node-centered finite volume scheme with a second order accuracy. The gas-liquid interface demarcates the volume boundaries where inner zone represents the condensed phase liquid fuel and outer zone represents the gas phase ambient and the far field (typically two hundred times the initial droplet diameter) is well defined using the Dirichlet conditions. The Dirichlet conditions imposed on the far-field are of fixed ambient composition and temperature (constant ambient composition $N_2/O_2 = 0.79/0.21$ and $T = 298$ K). The innermost liquid node is centered at the origin, providing the required no-flux condition. The liquid and gas phase mesh size for all the simulations for LLNL and MIT model are respectively 40 and 30, and 120 and 80. The hardware resources deployed for these simulations are Intel 16 CPU cores (2.4 GHz) with 96 GB of memory allocation. Typical simulation runtime of converged solution for LLNL and MIT model is respectively 50–53 CPU hours and 160–167 CPU hours.

The discretized mass flux is represented on cell interfaces and not cell centers, in the manner traditionally referred to as a staggered grid to avoid oscillatory solutions. Numerical integration of the final set of discretized equations is performed using a backward difference formula with a variable order of up to fifth order and a variable time step utilizing a fully implicit multipoint interpolation. This makes it appropriate for the large range of time scales and stability constraints imposed by chemically reacting systems when combined with automatic time-step variation. The gas phase domain is set as 200 times larger than the initial droplet size and the applied spark ignition energy input in the model is around 1 J, which is the lowest possible energy that numerically triggered a series of combustion reactions.

4. Results and discussion

Representative images from the droplet burning histories of different butanol isomers are shown in Fig. 3. The upper row in each box shows self-illuminated flame images that highlight the flame structure while the second rows are backlit images of the droplet boundary. Droplet flame of *n*-butanol (cf. Fig. 3a) maintained bluish flame almost all the time with the yellow glows caused by the fiber. The *iso*-butanol and *sec*-butanol droplet flame (cf. Fig. 3b and c) appears to produce a brighter yellow core among the four isomers that is enclosed by a pure blue zone. The flame produced by *tert*-butanol droplet (cf. Fig. 3d) is as bright as those produced by *iso*- and *sec*-butanol but that yellow core quickly dies out after 0.4 s. Though soot aggregates (i.e., a soot 'shell') were not visibly seen in the BW images, the yellow core could nonetheless suggest possible soot related intermediates that are consumed *in-situ* after

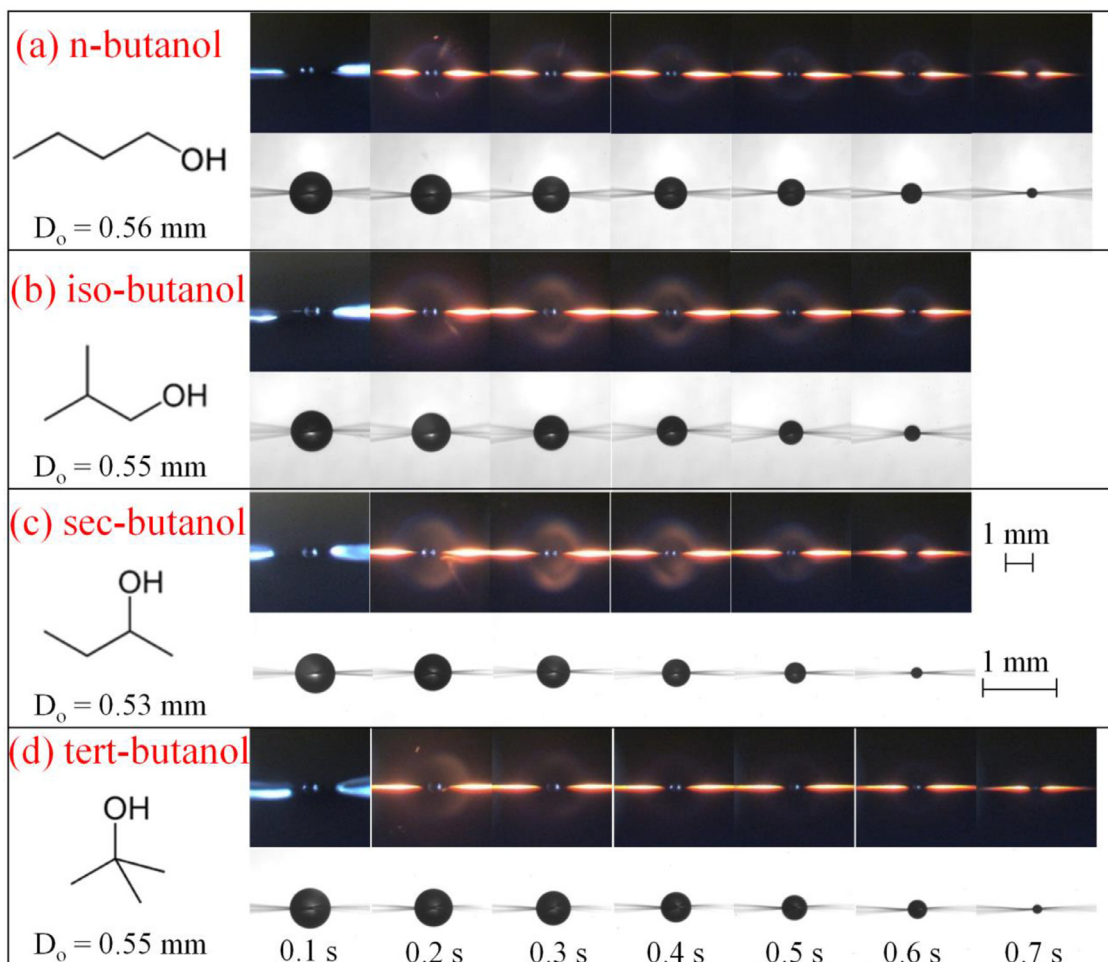


Fig. 3. Flame and droplet images obtained from droplet burning experiments for (a) *n*-butanol [52], (b) *iso*-butanol, (c) *sec*-butanol, (d) *tert*-butanol. The provided initial droplet diameters (D_0) pertain to the particular run.

they are being produced. The following discussion compares experimental data of droplet and flame diameters with DNM predictions.

Figure 4a includes the droplet burning histories (D^2 vs. time t , both scaled by the square of initial droplet diameter D_0^2) obtained from three individual experiments for each of the four butanol isomers. Four different colors, i.e. red, black, blue green are used in Fig. 4a and all the figures hereafter (except for the modeling results in Fig. 6) to represent different isomers. It is suggested in Fig. 4a that the experimental data are evidently very reproducible. Averaged data for each isomer are shown in Fig. 4b. The slopes of the data represent the droplet burning rate ($K = -d(D/D_0)^2/d(t/D_0^2)$). The evolutions of droplet diameter for *n*-, *iso*-, and *sec*-butanol are almost identical. The burning rate of *tert*-butanol is lower, which is believed not to be the result of the slightly smaller initial droplet diameter of *tert*-butanol compared to the other isomer droplets. The relative burning rates qualitatively correspond to the heat of combustion of the isomers (cf. Table 1): *tert*-butanol has the lowest heat of combustion (and lowest burning rates) among all isomers while the other three isomers have closer heat of combustion.

Figure 5 compares the evolution of D^2 from DNM predictions of the LLNL (dashed lines) and MIT (solid lines) kinetic models for all four isomers. The LLNL mechanism gives significantly higher burning rates (i.e., slopes of the lines in Fig. 5) for *iso*-, *sec*-, and *tert*-butanol compared to the MIT kinetics, while the MIT mechanism produces D^2 data that are more adjacent to each other. On the other hand, the D^2 evolution of *n*-butanol predicted by the LLNL and MIT kinetic models agree rather well with each other. The

general trend of predicted burning rates seems to be similar for both kinetics, i.e. $K_{tert} > K_{sec} > K_{iso} > K_n$. In this order, the predicted burning rate of *tert*-butanol is in the opposite trend of the experimental observation (cf. Fig. 4b): the data show that the burning rate of *tert*-butanol is significantly lower than that of the other isomers, while the predicted *tert*-butanol burning rate (Fig. 5) is higher. From perspective of the D^2 -law, it has been previously suggested that the burning rate (K) is proportional to a parameter $\zeta = k_g/(\rho_L C_{p,g})$ [59] where k_g is the thermal conductivity of gas, ρ_L is the liquid density, $C_{p,g}$ is the specific heat of gas. It is found that $C_{p,g}$ of *tert*-butanol is noticeably higher than those of other isomers from various sources including the thermal property data of the MIT model [43] and Ref. [5] in the range of 1200–1700 K, and therefore speculated to be a factor of *tert*-butanol's lowest burning rate. Note that the thermal property data appended to the LLNL model [40] produce almost the same values of $C_{p,g}$ for all four isomers. Therefore one should be careful while using the D^2 -law and physical properties to provide estimate of burning rates, especially for isomeric comparisons where values of physical properties are relatively close and slight variation from the model may lead to a different direction of discussions.

To provide clear comparisons with experimental results, Fig. 6a to d compares the predicted droplet diameters with measured values (cf. Fig. 4b) using the LLNL (dash red lines) and MIT (solid black lines) kinetic models. The experimental data shown in these plots include the error bars showing the standard deviations computed from three individual experiments (cf. Fig. 4a). For *n*-butanol

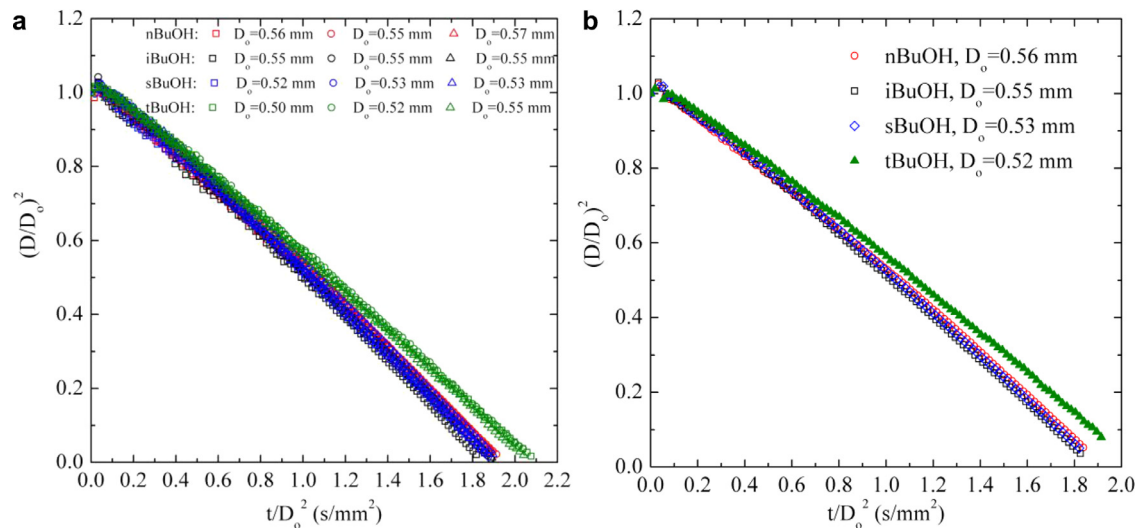


Fig. 4. Time-evolving droplet diameters measured from BW images for *n*-butanol [52], *iso*-butanol, *sec*-butanol, and *tert*-butanol: (a) three individual experiments for each butane isomers; (b) the average from (a) for each isomer. (For interpretation of the references to color in this figure legend, the reader is referred to the web version of this article.)

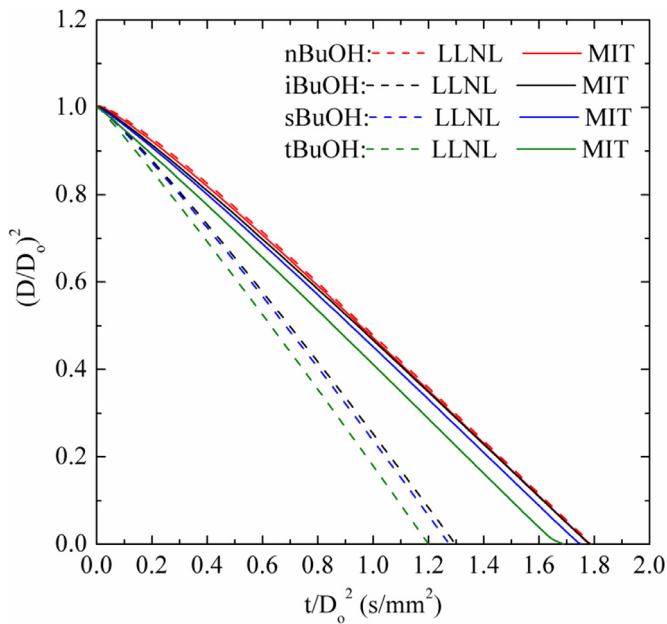


Fig. 5. Time-evolving droplet diameters predicted by numerical modeling (kinetics from Sarathy et al. [40] (LLNL, dashed line) and Merchant et al. [43] (MIT, solid line)) for all four butanol isomers. (For interpretation of the references to color in this figure legend, the reader is referred to the web version of this article.)

(Fig. 6a), the D^2 predictions using both models yielded similar burning curves with the absolute $(D/D_0)^2$ values slightly smaller than the experimental values. Though the absolute droplet diameter values from DNM are below the error bars, the slope (burning rates) near the end are very similar to experimental results. This would suggest that the slight discrepancy may stem from the earlier stage of the combustion process (i.e. $t/D_0^2 < 0.8$ s/mm²).

Figure 6b and c suggests that the MIT model better predicts the *iso*- and *sec*-butanol data compared to the LLNL model, which reflects the extensive validation of the MIT model with gas phase *sec*- and *iso*-butanol combustion properties. It is clear that the droplet diameters predicted using the LLNL model are significantly smaller than the measurements for *iso*-, *sec* and *tert*-butanol while predictions from the MIT model are better matched with the data (Fig. 6b–d). Furthermore, burning rates (slope of the data) pre-

dicted from the MIT kinetic model are in reasonable agreement with the experimental results for *iso*- and *sec*-butanol.

The numerical predictions for *tert*-butanol from both models (Fig. 6d) do not agree well with the data, though the MIT model is much closer to the measurements. Even considering validations of these kinetic models against premixed experimental combustion targets, both the LLNL and MIT models were found to not be in especially good agreement [20,21]. This suggests that there are possible limitations in the kinetic schemes due to limited insight into the mechanistic pathways associated with combustion of *tert*-butanol. Notably, from here onwards, the primary objective of this study will be to extensively investigate *sec*-, *iso*- and *tert*-butanol droplet combustion. Therefore subsequent discourse is mainly directed towards these isomers essentially precluding the already studied *n*-butanol [52].

The numerical predictions of instantaneous burning rate and peak gas temperature profiles for *sec*-, *iso*- and *tert*-butanol deploying both the chemical kinetic models are presented in Fig. 7. In addition, the droplet burning rate calculated from experimental dataset, delineated by solid symbol, is juxtaposed in respective subplots (Fig. 7a–c). As shown in the figure, predictions from Sarathy et al. (i.e. LLNL model) has consistently higher burning rate for all the isomers compared to Merchant et al. (i.e. MIT model) predictions. Interestingly, opposite to the experimental observation, there is no ‘quasi-steady’ burning period for the LLNL model. Instead, irrespective of the isomers, the model exhibits continuously increasing burning rate trend. All three isomers behave in a near-identical fashion with a sudden dip in the burning rate at the end indicating flame-out due to fuel depletion. In contrast, predictions from MIT model qualitatively regenerate the experimental profile and quantitatively reproduce the experimental observation, especially for *sec*- and *iso*-butanol though discrepancy is discernible for *tert*-butanol indicating faster burning rate. This also suggests that there is room for model refinement for the *tert*-butanol. A closer look into the *tert*-butanol burning rate also reveals that Merchant et al. predicts a flame extinction at the very last stage of the burn period.

In the same figure, subplots (d–f) illustrates a direct comparison of temporal evolution of peak gas temperature for both these models for three different isomers. Notably, for an individual isomer, respective simulations are performed under same level of initial ignition energy. It is perceptible from the figure that the LLNL model ignition chemistry for each of the isomers is

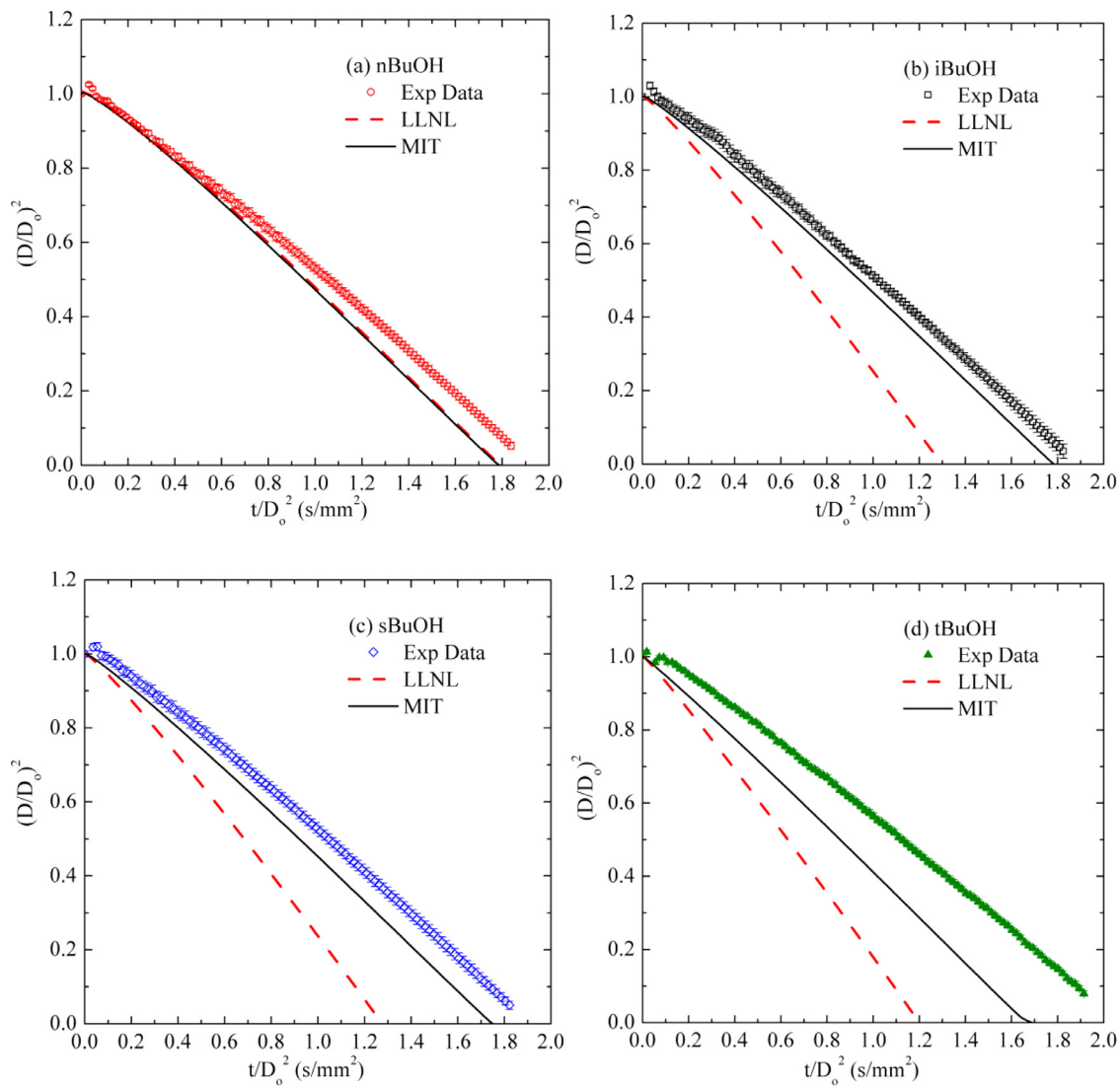


Fig. 6. Comparison of experimental data and numerical modeling results of droplet diameter regression for (a) *n*-butanol, (b) *iso*-butanol, (c) *sec*-butanol, (d) *tert*-butanol. The error bars on the symbols show are the standard deviations of individual runs (cf. Fig. 4a). Kinetics from Sarathy et al. [40] (LLNL, dash red line) and Merchant et al. [43] (MIT, black solid line). (For interpretation of the references to color in this figure legend, the reader is referred to the web version of this article.)

more sensitive than its counterpart model. Therefore, the rise in temperature for LLNL model is consistently earlier than that of MIT model. Surprisingly, immediately after the ignition transient, both the model approaches to the same maximum temperature throughout the life time of the burning droplet (i.e. at least till LLNL model predicted life time), both profiles remain almost the same except the flame-out phase. Given that the LLNL model prediction for average burning rate is approximately 50% higher than MIT prediction while both the models simulated the same peak gas temperature profile (until flame-out dynamics commences), possibly suggesting the LLNL flame location is positioned more outward radial position than MIT prediction. Thus, as a logical consequence, the following section includes the discussion on flame stand-off ratio. As MIT model is found to be a more accurate representation of butanol isomer kinetics against droplet combustion experiments, by implying comparison—it is discernible that all the butanol isomers produce near identical peak gas temperature profile indicative of similar flame/reaction zone temperature.

Figure 8a and b shows the evolution of FSR for butanol isomers in a similar fashion as in Fig. 4a and b, with 8a showing the data from all individual experiments and 8b the averaged data. No-

ticed from Fig. 8a that the *n*-butanol data are more scattered after $t/D_0^2 = 1.0$ s/mm² because it was slightly more difficult to pin point the flame boundary of the small bluish flame, especially in a dark background. In general, the data in Fig. 8a suggest that the FSR values from experiments are also very repeatable for each fuel. More clear trends of FSR can be found from the averaged data in Fig. 8b. It is evident that *n*-butanol has the lowest FSR along the combustion history. With the FSR of *sec*-butanol slightly higher than that of *iso*-butanol, *tert*-butanol exhibits the largest FSR among all four isomers. This ordering seems to remain throughout the droplet burning history. The continuously increasing FSR during the quasi-steady burn is primarily related to the far-field thermal buffering effect [63].

Figure 9 compares the FSR obtained from experiments and DNM predictions using both the LLNL and MIT models for *sec*-, *iso*- and *tert*-butanol. Two different approaches has been adopted for each model in defining the flame kernel position – (i) location of the peak gas-phase temperature (T_{max}), and (ii) location of the maximum heat release rate (HRR_{max}). The rationale in selecting these two quantities as FSR marker has already been substantiated elsewhere [52,63]. The experimental data are shown with an error

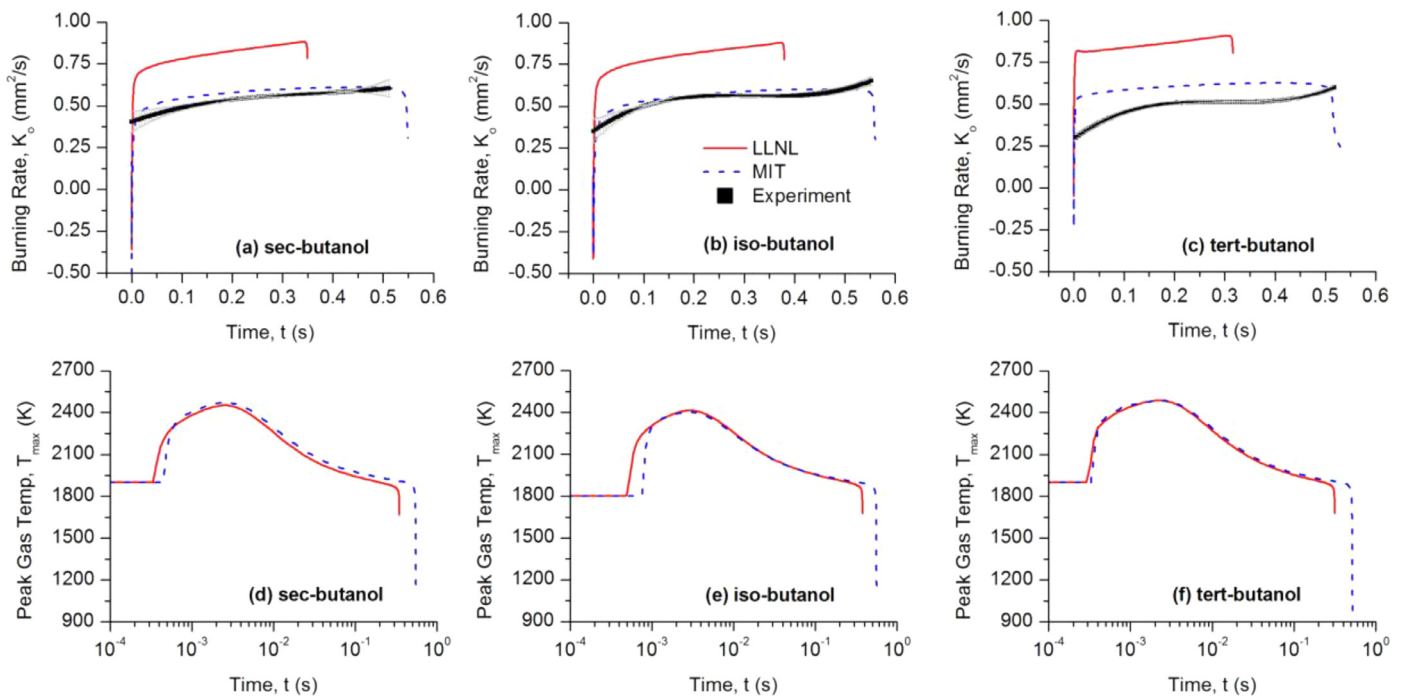


Fig. 7. Instantaneous burning rate (a–c) and peak gas temperature (d–f) comparison for Sarathy et al. [40] (LLNL, solid red) and Merchant et al. [43] (MIT, dashed blue) model for different butanol isomers. Subplot (a, d): *sec*-butanol, subplot (b, e): *iso*-butanol and subplot (c, f) *tert*-butanol. Instantaneous burning rate (top row): symbol (Black square) represents experiment data with associated error bars (gray). (For interpretation of the references to color in this figure legend, the reader is referred to the web version of this article.)

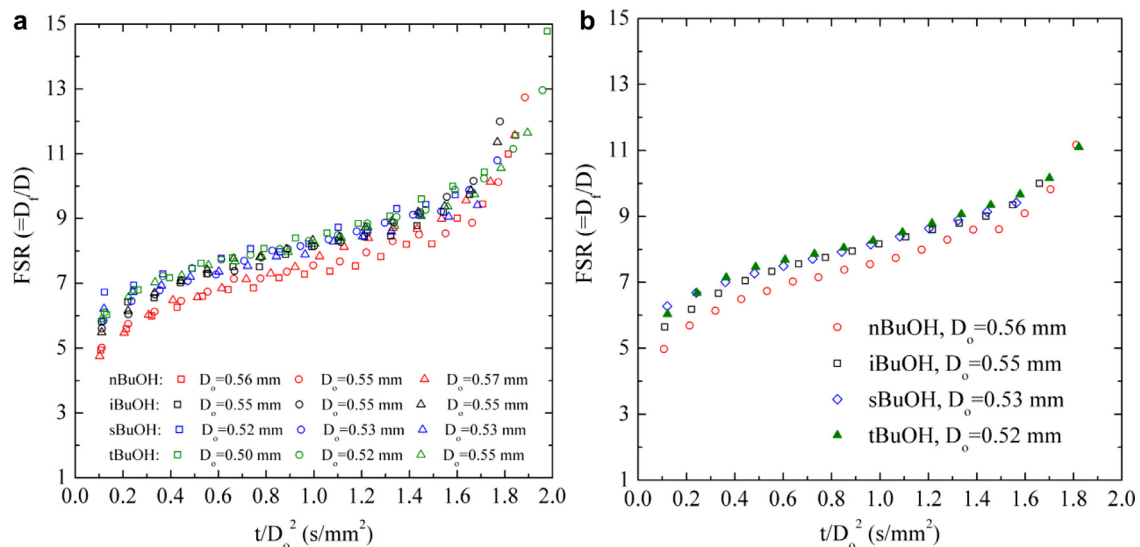


Fig. 8. Time-evolving flame standoff ratio (FSR) measured from experiments for *n*-butanol [52], *iso*-butanol, *sec*-butanol, and *tert*-butanol: (a) three individual experiments for each butane isomers; (b) the average from (a) for each isomer. (For interpretation of the references to color in this figure legend, the reader is referred to the web version of this article.)

bar representing the standard deviation from individual experiments. These error bars represents an uncertainty that is larger than the uncertainty from flame size measurements (8%) mentioned previously. It is discernible from the figure that irrespective of the butanol isomers, all of them show a similar trend in term of FSR evolution. By ignoring the initial ignition transient and flame out dynamics, their overall values evolve in between ~ 5.0 and 9.0 . Considering that the isomers are of similar initial diameters (0.54 ± 0.02 mm) and their FSR evolutions also remain same during the quasi-steady burning (inclusive of slope), it could be inferred that the flame experiences the same level of heat loss and reactant (fuel and/or pyrolyzed fuel fragments) gain from the flame

location. Initially, the droplet diameter (D) regresses linearly until (*sec*-/*iso*-/*tert*- $\sim 44\%/44\%/47\%$ of burn time) it starts to regress in nonlinear fashion. Part of this non-linear behavior is spurring from tether fiber additional thermal interaction, especially when the droplet is approaching the fiber diameter size [64]. Simultaneously, for the flame (not shown explicitly in the corresponding figure), it initially grows outwardly, reaches maximum and remains approximately fixed at around that location until the droplet enters the non-linear diameter regression time zone, and then the flame responds back to the shrinking droplet and decreases, albeit at a slower rate (i.e. slope) than the droplet [63]. This two coupled effect of droplet and flame causes the FSR to have an ever so slightly

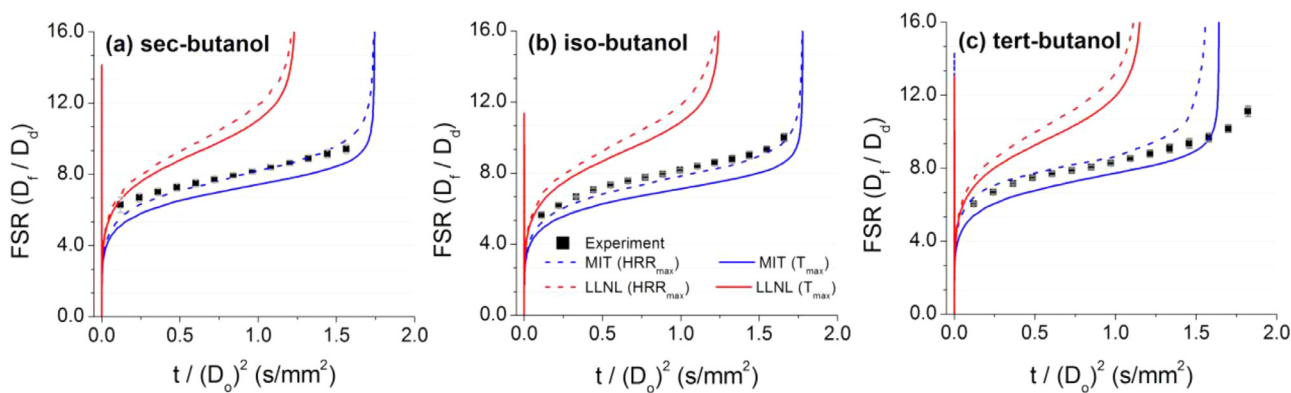


Fig. 9. Comparison of flame standoff ratio ($FSR = D_f/D_0$) from experiments (symbols) and numerical simulation [Red line: Sarathy et al. [40] (LLNL) and Blue line: Merchant et al. [43] (MIT)]. Solid line: flame diameter based on the location of peak gas phase temperature. Dashed line: flame diameter based on the location of maximum heat release rate. Subplot (a): *sec*-butanol, subplot (b): *iso*-butanol and subplot (c): *tert*-butanol. (For interpretation of the references to color in this figure legend, the reader is referred to the web version of this article.)

increasing pattern for all the isomers for such sub-millimeter size droplets. For *sec*-, *iso*- and *tert*-butanol isomers, the MIT model correctly simulated the FSR evolution, especially with HRR_{max} approach. Although the model's prediction capability is laudable for *sec*- and *iso*-butanol, slight disagreement for *tert*-butanol at the latter part of the burn time is noticeable. Surprisingly, for all the isomers reported here, LLNL model consistently over-predicts the FSR evolution from initial burn time with similar FSR trend throughout its burning period and ultimately exhibiting almost the same extinction/flame-out temporal location ($t/(D_0)^2 \sim 1.2\text{--}1.25\text{ s/mm}^2$).

The disparity in LLNL model predictions for FSR renders careful reexamination of the model itself. Both the FSR makers manifest that the flame reposition itself at a farther distance from the initial get-go. Intuitively, two possible explanation could be sought for – (i) inappropriate gas phase kinetics (i.e. rate constants) for isomer specific reactions, and/or (ii) faster transport coefficient. Inappropriate rate constant may possibly lead to excessive fuel decomposition that in turn may enhance excessive heat and temperature evolution. The excessive heat feedback drives the flame to reposition at a farther location which possibly explains the higher FSR. On the other hand, faster transport may disperse the reactive species (pure or decomposed fuel, intermediates and products) to the far field and also the reaction zone, resulting in higher FSR. In order to better comprehend the influence of the aforementioned two possibilities, spatial-temporal analysis of important parameters (temperature, species concentration etc.) are performed in the following section. Finally, at a latter part of the article, individual influence of thermodynamic properties, transport parameters and kinetic rate coefficients of isomer specific species for LLNL model are benchmarked against MIT counterpart model.

The spatial-temporal evolution of key species and temperature is illustrated in Figs. 10–11 for *tert*-butanol (and for *sec*- and *iso*-butanol in Supplementary Figures S1 and S2). It should be noted that the location of the flame (i.e. reaction zone) based on maximum temperature is delineated by the white dashed line in these plots. For the sake of direct comparison between the two models, predicted results are exhibited up to 0.3 s. It is clear from the figure that irrespective of the model, the fuel undergoes decomposition from near-surface location of the droplet. However, the radial zone over which the fuel decomposes (and subsequently disperses) as time progresses varies for individual model. According to MIT model, the fuel mass fraction completely vanishes to zero at approximately half the radial distance that is predicted by LLNL model. The extension of this analysis can be drawn towards the gas phase temperature and final products like carbon monoxide (CO) and carbon dioxide (CO₂). In congruence with earlier anal-

ysis, the temperature magnitude of both these models is almost the same including peak gas temperature (subplot 10b and 10d). However, the radial distribution significantly differs for both these model predictions. According to the LLNL model, the higher temperature field is diffused outward with time resulting in higher FSR whilst for the MIT model the high temperature section approaching a near-plateau after $\sim 0.1\text{ s}$, thus enabling FSR to increase ever so slightly compared to the LLNL model. Similar observation is rendered for final products like CO and CO₂. Although qualitative agreement is discernible for the mass fraction prediction for both these models, the radial spread of each of these species clearly demarcates the underlying differences between these two models. Spatial-temporal analysis for *sec*- and *iso*- butanol with similar conclusive observations are plotted and appended in the supplementary section.

The above description clearly highlights the difference between the two models when coupled with multiphase droplet combustion simulation. Intuitively, the disparity between the model predictions may stem from the variations in (i) elementary kinetic reactions and rate coefficients, (ii) thermodynamic property formulations and (iii) transport parameters. It is noteworthy that while the prime objective of the present study is to focus on the butanol isomer droplet combustion, the large prediction discrepancies between these two adopted models also require careful attention for the possible causes of deviation, notably for the LLNL model. The preceding discussion attempts to explore the contribution of three possible sources of deviation for the LLNL model. In this exercise, the previous simulation outcome of MIT model is considered as the base 'result' due to its better predictive capability against drop tower experiments. In actuality, both the models have different number of species and elementary reactions including difference in the fuel specific sub-model (e.g. bimolecular reactions for isomer decomposition). To check whether the prediction difference is occurring from thermodynamic or transport property variation, isomer specific common species of LLNL is exchanged with MIT model data. Similarly, common reactions (isomer specific) are interchanged with the MIT model. It should be noted that other species and reactions are not modified in accordance with MIT model. As the main skeletal of the LLNL model comprise the *n*-butanol reaction kinetics, and the model exhibits good predictability for *n*-butanol [52], therefore other species and reactions are not interchanged with MIT model as well. Subsequently, three individual runs are performed and reported in Fig. 12 along with experimental measurement only for *tert*-butanol droplet combustion. As evident in Fig. 12, reaction kinetics and thermodynamic expression exchange does not contribute to distinguishable difference than its

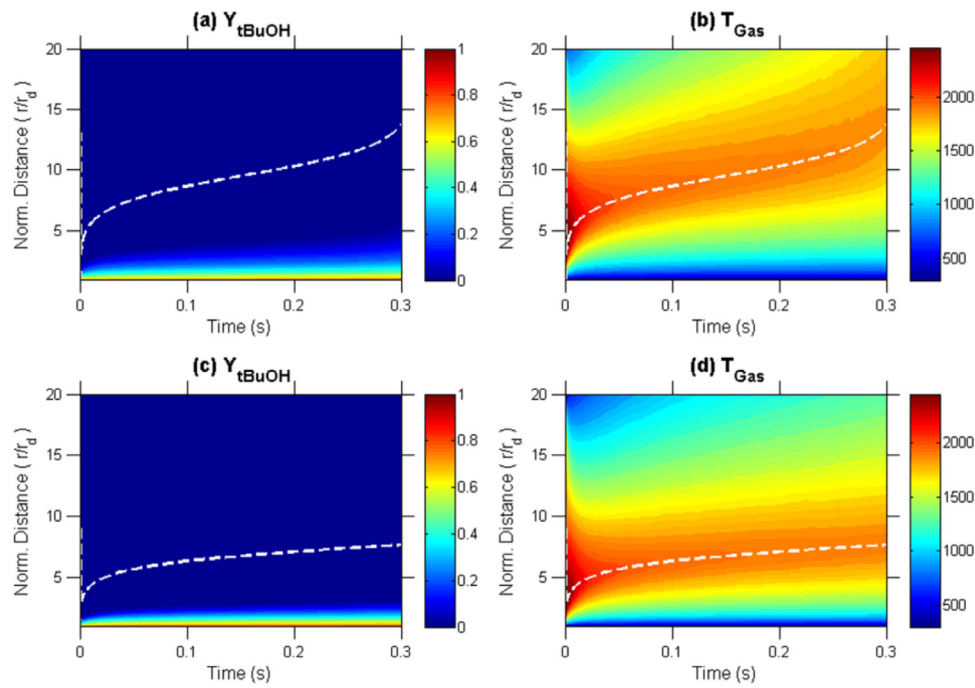


Fig. 10. Spatial-temporal evolution of *tert*-butanol mass fraction ($Y_{t\text{BuOH}}$: subplot a, c) and gas phase temperature (T_{gas} : subplot b, d) for *tert*-butanol droplet combustion. Top row: Sarathy et al. [40] (LLNL), bottom row: Merchant et al. [43] (MIT). Dashed line (white): Computationally evaluate flame location based on maximum temperature location. Results are reported up to 0.3 s for common comparison.

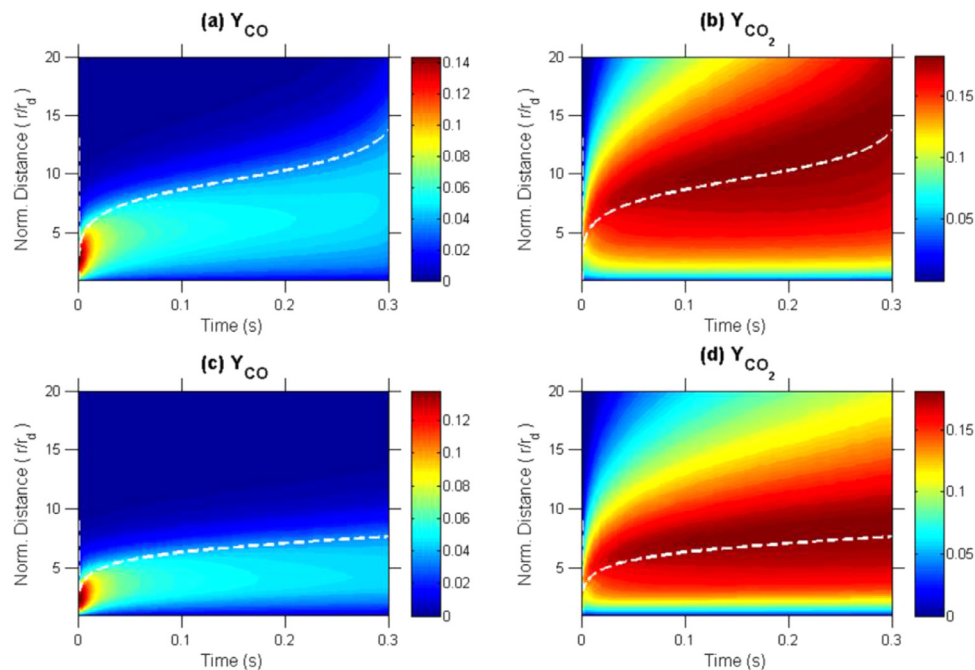


Fig. 11. Spatial-temporal evolution of carbon monoxide mass fraction (Y_{CO} : subplot a, c) and carbon dioxide mass fraction (Y_{CO_2} : subplot b, d) for *tert*-butanol droplet combustion. Top row: Sarathy et al. [40] (LLNL), bottom row: Merchant et al. [43] (MIT). Dashed line (white): Computationally evaluate flame location based on maximum temperature location. Results are reported up to 0.3 s for common comparison.

base run reported earlier (cf. Fig. 6, 7, and 9). However, for the case of transport property data exchange, the LLNL model prediction reproduces the model prediction of MIT model. This also explains the wider dispersion of species and temperature field as illustrated in Fig. 10 and supplementary Fig. S1 and S2 even though the peak gas temperature are found to be near-identical (cf. Fig. 7).

Finally, the experimental flame imaging, as illustrated in Fig. 3, provides a vital lead in investigating the sooting tendency of butanol isomer droplets at atmospheric pressure. It is evident that

with the exception of *n*-butanol flame, *iso*-, *sec*- and *tert*-butanol flame exhibited visibly prominent yellow luminosity between the outer flame boundary (pale bluish) and the inner droplet surface. The luminosity for *tert*-butanol monotonically vanishes as the droplet regresses, whereas it continues to be observed for *sec*- and *iso*-butanol until the droplet reaches its flame-out. Interestingly, even though the yellow flame is a classical ‘observatory’ marker for soot, no subsequent soot shell (and/or soot fragment) was experimentally ever noticed which indirectly suggests that

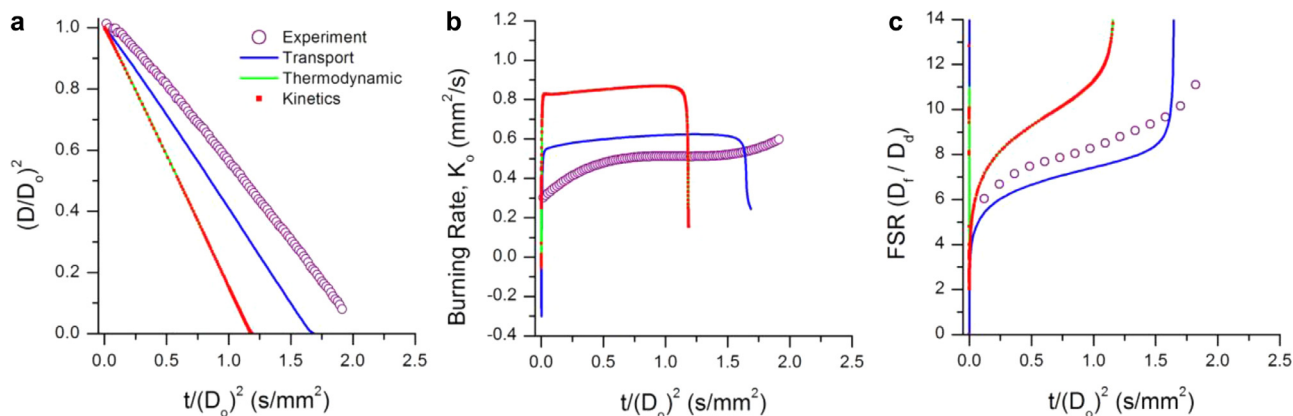


Fig. 12. Effect of transport parameter, thermodynamic property formulations and elementary kinetic reactions for Sarathy et al. [40] (LLNL) model for *tert*-butanol droplet combustion on (a) droplet regression (b) burning rate and (c) flame stand-off ratio. Blue line: isomer specific species transport data exchanged with Merchant et al. [43] (MIT) model. Green line: isomer specific species thermodynamic data exchanged with MIT model. Red square (small) symbol: isomer specific elementary reactions exchanged with MIT model. (For interpretation of the references to color in this figure legend, the reader is referred to the web version of this article.)

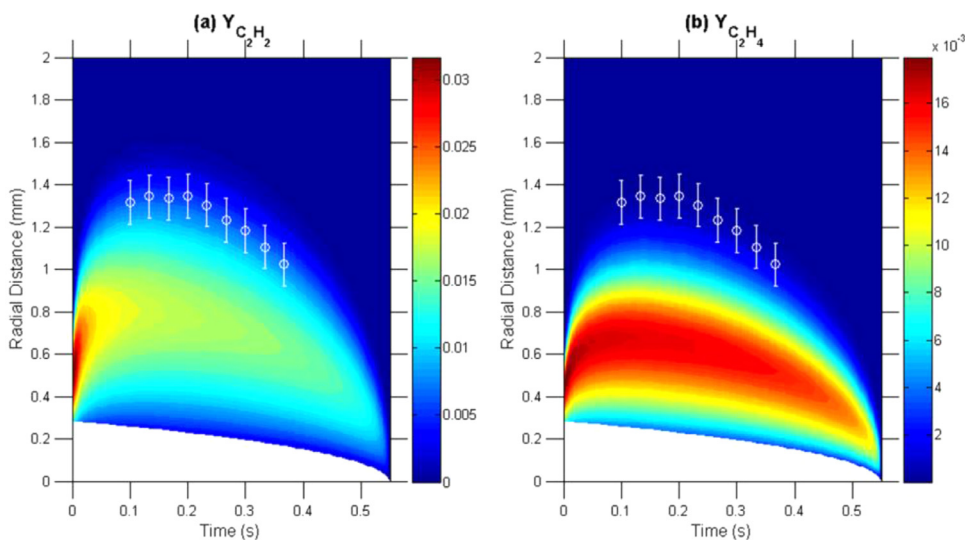


Fig. 13. Spatial-temporal evolution of mass fraction of (a) Acetylene, C_2H_2 , (b) Ethylene, C_2H_4 for *sec*-butanol droplet combustion deploying Merchant et al. [43] (MIT) model. Symbol (diamond): experimentally measured flame radii (with time) and associated uncertainties.

the mechanism leading to soot oxidation is also competitive to soot production. This speculation is further explored by invoking spatial-temporal analysis of key soot precursor like acetylene (C_2H_2) and ethylene (C_2H_4). The analysis is limited to *sec*- and *iso*-butanol for the simulations involving MIT model only. As the current droplet modeling platform model does not include a comprehensive soot modeling module, the forth-coming discourse should be parsed carefully as a ‘qualitative’ analysis to comprehend the gross features as observed in the experiments.

The mass fraction of soot precursors, i.e. C_2H_2 and C_2H_4 , are plotted in space-time coordinates for *sec*- and *iso*-butanol in Figs. 13 and 14 respectively. Experimental evolution of the outer flame edge radii (with time) along with associated experimental uncertainties is collocated in the figures for visual reference of the flame position. Similar to the experimental observation for the ‘yellow luminosity’, computational predictions of mass fractions for C_2H_2 and C_2H_4 (for both the isomers) also evolved within the experimentally measured outer flame radius. Moreover, the mass fraction concentration peaks in between the droplet surface and the outer flame region. And subsequently, $Y_{C_2H_2}$ or $Y_{C_2H_4}$ reduces to zero near the experimentally measured flame location which qualitatively manifests the hypothesis of soot oxidation within the physical flame boundary. Intuitively, this indirectly ratifies the

business of the MIT model, even though no soot modeling was coupled with the existing computational effort.

5. Conclusions

Experimental results of droplet burning obtained under conditions that promote spherical droplet flames show that D^2 histories of *n*-, *iso*-, and *sec*-butanol are almost identical while *tert*-butanol has noticeably lower burning rates. FSR results suggest that *n*-butanol has the smallest FSR with the other three butanol isomers having FSRs close to each other. The experimentally observed trend for FSR is $FSR_{tert} > FSR_{sec} > FSR_{iso} > FSR_n$.

The experimental measurements are compared with DNM predictions using detailed combustion chemistries reported by LLNL and MIT. The LLNL model does a good job predicting the D^2 and FSR of *n*-butanol, but it overshoots the burning rates and FSRs of the other three isomers. The MIT model best predicts the evolution of droplet diameter for *iso*-butanol and provides acceptable predictions for the other isomers.

While DNM using the MIT model offers fairly good agreement with data for *iso*-, *sec*- and *tert*-butanol, it still tends to slightly overestimate the FSRs. The predictions for *tert*-butanol from either LLNL or MIT model are not as aligned with the data as for

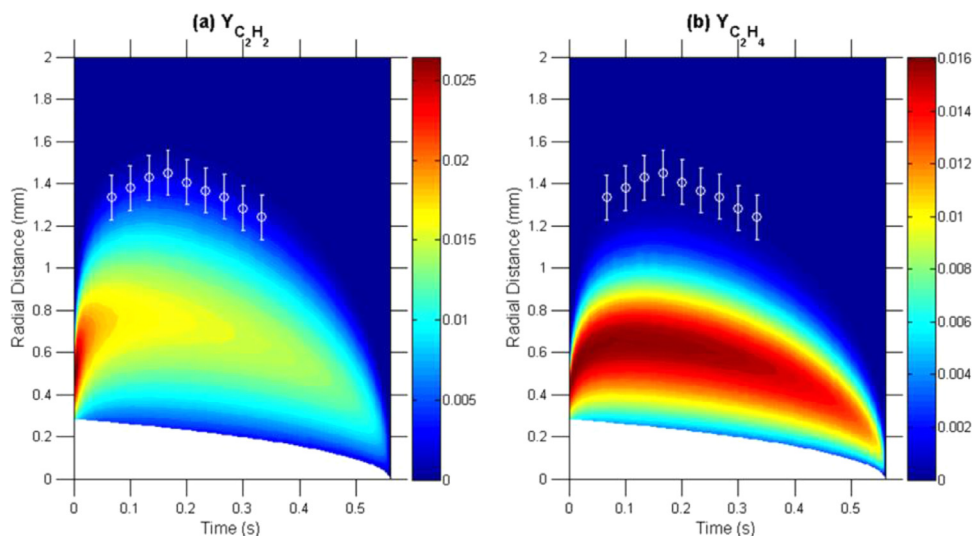


Fig. 14. Spatial-temporal evolution of mass fraction of (a) Acetylene, C_2H_2 , (b) Ethylene, C_2H_4 for *iso*-butanol droplet combustion deploying Merchant et al. [43] (MIT) model. Symbol (diamond): experimentally measured flame radii (with time) and associated uncertainties.

the other isomers which suggests room for improvement in the future.

Finally, the influence of chemical kinetics, thermodynamic and transport properties of Sarathy et al model (LLNL) for droplet combustion is individually analyzed. The rigorous computational analysis highlights that the difference in transport property coefficients of isomer specific species for LLNL model is responsible for the deviations observed for droplet combustion experiments. A reexamination of updated transport parameters for the LLNL model is thus suggested.

Acknowledgments

The authors acknowledge the National Aeronautics and Space Administration (NASA) for their financial support through grants No. NNX08AI51G (for YCL, YX, and CTA), NNX09AW19A (for FLD), and NNX14AG461A (for FEA and TF). The simulation work is also supported by the Startup Fund of University of South Carolina (for FEA and TD). The authors thank their project monitors Daniel Dietrich and Michael Hicks of NASA for helpful discussions, as well as the other FLEX2 team members (Forman Williams of UC-San Diego, Ben Shaw of UC-Davis, and Mun Choi of U-Conn) for their interest in our work.

Supplementary materials

Supplementary material associated with this article can be found, in the online version, at [doi:10.1016/j.combustflame.2016.04.018](https://doi.org/10.1016/j.combustflame.2016.04.018).

References

- [1] Transforming Combustion Research Through Cyberinfrastructure, Committee on Building Cyberinfrastructure for Combustion Research, National Research Council, The National Academies Press, April 2011 ISBN-13: 978-0-309-16387-3. http://www.nap.edu/catalog.php?record_id=13049.
- [2] Biofuels 2020, A policy driven logistics and business challenge. Research and innovation, position paper 02, 2010. Available at: http://www.dnv.com/binaries/biofuels%202020%20position%20paper_tcm4-434417.pdf
- [3] Carbon disclosure project transport report. Analysis based on CDP 2009 data. Available at: <https://www.cdp.net/CDPResults/CDP-Transport-Report.pdf>.
- [4] P.S. Nigam, A. Singh, Production of liquid biofuels from renewable resources, *Prog. Energy Combust. Sci.* 37 (2011) 52–68.
- [5] R.C. Reid, J.M. Prausnitz, T.K. Sherwood, The properties of gases and liquids, 3rd edition, McGraw-Hill, 1977, p. 642. Appendix A.
- [6] C. Jin, M. Yao, H. Liu, C. Lee, J. Ji, Progress in the production and application of *n*-butanol as a biofuel, *Renew. Sustain. Energy Rev* 15 (2011) 4080–4106.
- [7] H.A. Skinner, A. Sneison, The heats of combustion of the four isomeric butyl alcohols, *Trans. Faraday Soc.* 56 (1960) 1776–1783.
- [8] T. Wallner, R. Frazee, Study of regulated and non-regulated emissions from combustion of gasoline, alcohol fuels and their blends in a DI-SI Engine, SAE Technical Paper 2010-01-1571, 2010.
- [9] B.G. Harvey, H.A. Meylemans, The role of butanol in the development of sustainable fuel technologies, *J. Chem. Technol. Biotechnol.* 86 (2011) 2–9.
- [10] D.C. Rakopoulos, C.D. Rakopoulos, E.G. Giakoumis, A.M. Dimaratos, D.C. Kyritsis, Effects of butanol–diesel fuel blends on the performance and emissions of a high-speed DI diesel engine, *Energy Convers. Manage.* 51 (2010) 1989–1997.
- [11] T. Wallner, S.A. Miers, S. McConnell, A comparison of ethanol and butanol as oxygenates using a direct-injection, spark-ignition engine, *J. Eng. Gas Turbine Power* 131 (2009) 032802.
- [12] X. Gu, Z. Huang, J. Cai, X. Wu, C. Lee, Emission characteristics of a spark-ignition engine fuelled with gasoline–*n*-butanol blends in combination with EGR, *Fuel* 93 (2012) 611–617.
- [13] O. Doğan, The influence of *n*-butanol/diesel fuel blends utilization on a small diesel engine performance and emissions, *Fuel* 90 (2011) 2467–2472.
- [14] L. Siwale, L. Kristóf, T. Adam, A. Bereczky, M. Mbarawa, A. Penninger, A. Koiesnikov, Combustion and emission characteristics of *n*-butanol/diesel fuel blend in a turbo-charged compression ignition engine, *Fuel* 107 (2013) 409–418.
- [15] Z. Chen, Z. Wu, J. Liu, C. Lee, Combustion and emissions characteristics of high *n*-butanol/diesel ratio blend in a heavy-duty diesel engine and EGR impact, *Energy Convers. Manage.* 78 (2014) 787–795.
- [16] M. Zheng, X. Han, U. Asad, J. Wang, Investigation of butanol-fuelled HCCI combustion on a high efficiency diesel engine, *Energy Convers. Manage.* 98 (2015) 215–224.
- [17] R.K. Maurya, A.K. Agarwal, Combustion and emission characterization of *n*-butanol fueled HCCI engine, *J. Energy Res. Technol.* 137 (2015) 011101.
- [18] C. Regalbuto, M. Pennisi, B. Wigg, D. Kyritsis, Experimental investigation of butanol isomer combustion in spark ignition engines, SAE Technical Paper 2012-01-1271, 2012.
- [19] K. Fushimi, E. Kinoshita, Y. Yoshimoto, Effect of butanol isomer on diesel combustion characteristics of butanol/gas oil blend, SAE Technical Paper 2013-32-9097, 2013.
- [20] C.S. McEnally, L.D. Pfefferle, Fuel decomposition and hydrocarbon growth processes for oxygenated hydrocarbons: butyl alcohols, *Proc. Combust. Inst.* 30 (2005) 1363–1370.
- [21] B. Yang, P. Oßwald, Y. Li, J. Wang, L. Wei, Z. Tian, F. Qi, K. Kohse-Höinghaus, Identification of combustion intermediates in isomeric fuel-rich premixed butanol–oxygen flames at low pressure, *Combust. Flame* 148 (2007) 198–209.
- [22] P. Dagaut, C. Togbé, Experimental and modeling study of the kinetics of oxidation of butanol–*n*-heptane mixtures in a jet-stirred reactor, *Energy Fuels* 23 (2009) 3527–3535.
- [23] S.M. Sarathy, M.J. Thomson, C. Togbé, P. Dagaut, F. Halter, C. Mounaim-Rousselle, An experimental and kinetic modeling study of *n*-butanol combustion, *Combust. Flame* 156 (2009) 852–864.
- [24] S.M. Sarathy, M.J. Thomson, C. Togbé, P. Dagaut, F. Halter, C. Mounaim-Rousselle, Corrigendum to “An experimental and kinetic modeling study of *n*-butanol combustion” [Combust. Flame 156 (2009) 852–864], *Combust. Flame* 157 (2010) 837–838.
- [25] A. Frassoldati, R. Grana, T. Faravelli, E. Ranzi, P. Oßwald, K. Kohse-Höinghaus, Detailed kinetic modeling of the combustion of the four butanol isomers in premixed low-pressure flames, *Combust. Flame* 159 (2012) 2295–2311.

- [26] J.T. Moss, A.M. Berkowitz, M.A. Oehlschlaeger, J. Biet, V. Warth, P. Glaude, F. Battin-Leclerc, An experimental and kinetic modeling study of the oxidation of the four isomers of butanol, *J. Phys. Chem. A* 112 (2008) 10843–10855.
- [27] G. Black, H.J. Curran, S. Pichon, J.M. Simme, V. Zhukov, Bio-butanol: combustion properties and detailed chemical kinetic model, *Combust. Flame* 157 (2010) 363–373.
- [28] I. Stranic, S.H. Pyun, D.F. Davidson, R.K. Hanson, Multi-species measurements in 2-butanol and *i*-butanol pyrolysis behind reflected shock waves, *Combust. Flame* 160 (2013) 1012–1019.
- [29] I. Stranic, D.P. Chase, J.T. Harmon, S. Yang, D.F. Davidson, R.K. Hanson, Shock tube measurements of ignition delay times for the butanol isomers, *Combust. Flame* 159 (2012) 516–527.
- [30] B.W. Weber, K. Kumar, Y. Zhang, C.-J. Sung, Autoignition of *n*-butanol at elevated pressures and low-to-intermediate temperature, *Combust. Flame* 158 (2011) 809–819.
- [31] D.M.A. Karwat, S.W. Wagnon, P.D. Teini, M.S. Wooldridge, On the chemical kinetics of *n*-butanol: ignition and speciation studies, *J. Phys. Chem. A* 115 (2011) 4909–4921.
- [32] P.S. Veloo, F.N. Eglolfopoulos, Flame propagation of butanol isomers/air mixtures, *Proc. Combust. Inst.* 33 (2011) 987–993.
- [33] R. Grana, A. Frassoldati, T. Faravelli, U. Niemann, E. Ranzi, R. Seiser, R. Cattolica, K. Seshadri, An experimental and kinetic modeling study of combustion of isomers of butanol, *Combust. Flame* 157 (2010) 2137–2154.
- [34] J.K. Lefkowitz, J.S. Heyne, S.H. Won, S. Dooley, H.H. Kim, F.M. Haas, S. Jahangirian, F.L. Dryer, Y. Ju, A chemical kinetic study of tertiary-butanol in a flow reactor and a counterflow diffusion flame, *Combust. Flame* 159 (2012) 968–978.
- [35] T.S. Norton, F.L. Dryer, The flow reactor oxidation of C1–C4 alcohols and MTBE, *Symp. (Int.) Combust.* 23 (1991) 179–185.
- [36] J. Cai, L. Zhang, J. Yang, Y. Li, L. Zhao, F. Qi, Experimental and kinetic modeling study of *tert*-butanol combustion at low pressure, *Energy* 43 (2012) 94–102.
- [37] J. Cai, L. Zhang, F. Zhang, Z. Wang, Z. Cheng, W. Yuan, F. Qi, Experimental and kinetic modeling study of *n*-butanol pyrolysis and combustion, *Energy Fuels* 26 (2012) 5550–5568.
- [38] P. Oßwald, H. Guldenberg, K. Kohse-Höinghaus, B. Yang, T. Yuan, F. Qi, Combustion of butanol isomers – a detailed molecular beam mass spectrometry investigation of their flame chemistry, *Combust. Flame* 158 (2011) 2–15.
- [39] O. Welz, J.D. Savee, A.J. Eskola, L. Sheps, D.L. Osborn, C.A. Taatjes, Low-temperature combustion chemistry of biofuels: pathways in the low-temperature (550–700 K) oxidation chemistry of isobutanol and *tert*-butanol, *Proc. Combust. Inst.* 34 (2013) 493–500.
- [40] S.M. Sarathy, S. Vranckx, K. Yasunaga, M. Mehl, P. Oßwald, W.K. Metcalfe, C.K. Westbrook, W.J. Pitz, K. Kohse-Höinghaus, R.X. Fernandes, H.J. Curran, A comprehensive chemical kinetic combustion model for the four butanol isomers, *Combust. Flame* 159 (2012) 2028–2055.
- [41] K.M. Van Geem, S.P. Pyl, G.B. Martin, M.R. Harper, W.H. Green, Accurate high-temperature reaction networks for alternative fuels: butanol isomers, *Ind. Eng. Chem. Res.* 49 (2010) 10399–10420.
- [42] M.R. Harper, K.M. Van Geem, S.P. Pyl, G.B. Marin, W.H. Green, Comprehensive reaction mechanism for *n*-butanol pyrolysis and combustion, *Combust. Flame* 158 (2011) 16–41.
- [43] S.S. Merchant, E.F. Zanoelo, R.L. Speth, M.R. Harper, K.M. Van Geem, W.H. Green, Combustion and pyrolysis of *iso*-butanol: experimental and chemical kinetic modeling study, *Combust. Flame* 160 (2013) 1907–1929.
- [44] M.E. Baumgardner, S.M. Sarathy, A.J. Marchese, Autoignition characterization of primary reference fuels and *n*-heptane/*n*-butanol mixtures in a constant volume combustion device and homogeneous charge compression ignition engine, *Energy Fuels* 27 (2013) 7778–7789.
- [45] W. Liu, A.P. Kelley, C.K. Law, Non-premixed ignition, laminar flame propagation, and mechanism reduction of *n*-butanol, *iso*-butanol, and methyl butanoate, *Proc. Combust. Inst.* 33 (2011) 995–1002.
- [46] T.F. Lu, C.K. Law, Toward accommodating realistic fuel chemistry in large-scale computations, *Prog. Energy Combust. Sci.* 35 (2009) 192–215.
- [47] H. Wang, R.D. Reitz, M. Yao, B. Yang, Q. Jiao, L. Qiu, Development of an *n*-heptane-*n*-butanol-PAH mechanism and its application for combustion and soot prediction, *Combust. Flame* 160 (2013) 504–519.
- [48] Y.C. Liu, A.J. Savas, C.T. Avedisian, The spherically symmetric droplet burning characteristics of Jet-A and biofuels derived from camelina and tallow, *Fuel* 108 (2013) 824–832.
- [49] K.-L. Pan, M.-C. Chiu, Droplet combustion of blended fuels with alcohol and biodiesel/diesel in microgravity condition, *Fuel* 113 (2013) 757–765.
- [50] T.I. Farouk, Y.C. Liu, A.J. Savas, C.T. Avedisian, F.L. Dryer, Sub-millimeter sized methyl butanoate droplet combustion: microgravity experiments and detailed numerical modeling, *Proc. Combust. Inst.* 34 (2013) 1609–1616.
- [51] Y.C. Liu, T. Farouk, A.J. Savas, F.L. Dryer, C.T. Avedisian, On the spherically symmetrical combustion of methyl decanoate droplets and comparisons with detailed numerical modeling, *Combust. Flame* 160 (2013) 641–655.
- [52] F.E. Alam, Y.C. Liu, C.T. Avedisian, F.L. Dryer, T.I. Farouk, *n*-Butanol droplet combustion: numerical modeling and reduced gravity experiments, *Proc. Combust. Inst.* 35 (2015) 1693–1700.
- [53] Y. Xu, C.T. Avedisian, Combustion of *n*-butanol, gasoline, and *n*-butanol/gasoline mixture droplets, *Energy Fuels* 29 (2015) 3467–3475.
- [54] G.A. Agoston, B.J. Wood, H. Wise, Influence of pressure on the combustion of liquid spheres, *J. Jet Propul.* 28 (1958) 181–188.
- [55] Y. Ogami, S. Sakurai, S. Hasegawa, M. Jangi, H. Nakamura, K. Yoshinaga, H. Kobayashi, Microgravity experiments of single droplet combustion in oscillatory flow at elevated pressure, *Proc. Combust. Inst.* 32 (2009) 2171–2178.
- [56] C.H. Wang, C.K. Law, Microexplosion of fuel droplets under high pressure, *Combust. Flame* 59 (1985) 53–62.
- [57] S. Nakaya, K. Fujishima, M. Tsue, M. Kono, D. Segawa, Effects of droplet diameter on instantaneous burning rate of isolated fuel droplets in argon-rich or carbon dioxide-rich ambiances under microgravity, *Proc. Combust. Inst.* 34 (2013) 1601–1608.
- [58] C.K. Law, T.Y. Xiong, C.H. Wang, Alcohol droplet vaporization in humid air, *Int. J. Heat Mass Transfer* 30 (1987) 1435–1443.
- [59] Y.C. Liu, C.T. Avedisian, A comparison of the spherical flame characteristics of sub-millimeter droplets of binary mixtures of *n*-heptane/*iso*-octane and *n*-heptane/toluene with a commercial unleaded gasoline, *Combust. Flame* 159 (2012) 770–783.
- [60] Y.C. Liu, A.J. Savas, C.T. Avedisian, Comparison of the burning characteristics of indolene and commercial grade gasoline droplets without convection, *Energy Fuels* 26 (2012) 5740–5749.
- [61] Y.C. Liu, Y. Xu, C.T. Avedisian, M.C. Hicks, The effect of support fibers on micro-convection in droplet combustion experiments, *Proc. Combust. Inst.* 35 (2015) 1709–1716.
- [62] C.L. Dembia, Y.C. Liu, C.T. Avedisian, Automated data analysis for consecutive images from droplet combustion experiments, *Image Anal. Stereol.* 31 (2012) 137–148.
- [63] T. Farouk, F.L. Dryer, Microgravity droplet combustion: effect of tethering fiber on burning rate and flame structure, *Combust. Theor. Model.* 15 (2011) 487–515.
- [64] T.I. Farouk, F.L. Dryer, On the extinction characteristics of alcohol droplet combustion under microgravity conditions – a numerical study, *Combust. Flame* 159 (2012) 3208–3223.
- [65] T.E. Daubert, R.P. Danner, H.M. Sibul, C.C. Stebbins, Physical and thermodynamic properties of pure chemicals: data compilation, Taylor and Francis, Bristol, PA, 1989.